Defence Technology 17 (2021) 234–244

Contents lists available at ScienceDirect

Defence Technology

journal homepage: www.keaipublishing.com/en/journals/defence-technology

Mechanical properties and thermal conductivity of pristine and functionalized carbon nanotube reinforced metallic glass composites: A molecular dynamics approach

Sumit Sharma*, S.K. Tiwari, Sagar Shakya

Department of Mechanical Engineering, Dr. B. R. Ambedkar National Institute of Technology, Jalandhar, India

ARTICLE INFO

Article history:
Received 31 January 2020
Received in revised form
6 March 2020
Accepted 1 April 2020
Available online 10 April 2020

Keywords:
Molecular dynamics
Carbon nanotube
Metallic glass
Mechanical properties
Thermal conductivity

ABSTRACT

This work uses the molecular dynamics approach to study the effects of functionalization of carbon nanotubes (CNTs) on the mechanical properties of $Cu_{64}Zr_{36}$ metallic glass (MG). Three types of functional groups, carboxylic, vinyl and ester were used. The effect of CNT volume fraction (V_f) and the number of functional groups attached to CNT, on the mechanical properties and thermal conductivity of CNT-MG composites was analysed using Biovia Materials Studio. At lower values of V_f (from 0 to 5%), the percentage increase in Young's modulus was approximately 66%. As the value of V_f was increased further (from 5 to 12%), the rate of increase in Young's modulus was reduced to 16%. The thermal conductivity was found to increase from 1.52 W/mK at $V_f = 0\%$ to 5.88 W/mK at $V_f = 12\%$, thus giving an increase of approximately 286%. Functionalization of SWCNT reduced the thermal conductivity of the SWCNT-MG composites.

1. Introduction

This study deals with the carbon nanotube (CNT) reinforced metallic glass (MG) nanocomposites. We always need a material which can perform efficiently without any external stimulus not only at elevated temperature but even at cryogenic temperatures. Such a requirement has always encouraged scientists to experiment with materials of all classes. Materials used in rovers for space exploration have to undergo similar conditions where the temperature difference during day and night can reach over 100 °C. The materials needed for such applications are expected to exhibit near-zero thermal expansion coefficients while retaining all of its mechanical properties. Borosilicates, quartz and other glasses have been proposed for their superior thermal properties, but their performance under exerted mechanical loads was found to be unsatisfactory. Metals are generally crystalline. MGs are prepared by cooling a metallic liquid so rapidly such that crystallization is avoided and the atoms have no time to arrange themselves into a crystalline lattice. In 1960 first MG of $Au_{75}Si_{25}$ was discovered by Klement et al. at California Institute of Technology, the USA by Klement et al. [1]. MG is defined as a material having a highly amorphous structure similar to that of liquids. High cooling rates, as high as 10^5–10^6 K/s are generally required for avoiding crystallization and the formation of MG. Compared to conventional metals and metal alloys, MGs have extraordinary mechanical properties. This mainly stems from the lack of crystalline structure due to which there are no crystal defects, i.e. point defects, line defects, etc. resulting in very high strength, toughness, and elasticity. Also, there are no grain boundaries due to which the corrosion resistance and wear resistance is superior as compared to conventional metals alloys. BMG has several applications. These include micro-electromechanical systems (MEMS), nano-electromechanical systems (NEMS), bio-medical implants, surgical tools, and micro-machines. BMGs have high values of Young's modulus and elastic strain. These also have high formability in the super-cooled liquid region.

These properties have resulted in the usage of BMG alloys for the fabrication of components with complex shapes such as gears and coiled springs. BMG alloys have been considered as the most suitable material for fuel-cell separators. Recently, NASA has demonstrated the use of BMG for making gears for robots which can be used at temperatures as low as −150 °C. The gears made from BMG

* Corresponding author.
E-mail address: sharmas@nitj.ac.in (S. Sharma).
Peer review under responsibility of China Ordnance Society

https://doi.org/10.1016/j.dt.2020.04.004

do not require any heating of grease used in gears. The surface temperature of Mars and that of Jupiter's moon-Titan is around −100 °C. At such low temperatures, the grease on gears has to be heated up before their usage. This consumes a substantial amount of energy. Thus BMG can be the materials for gears used in space and defence applications. Also, the military aircrafts used in high altitude regions have to withstand temperatures as low as −50 °C. At such low temperatures, ductile to brittle transition (DBT) takes place which causes brittle failure. To prevent this, CNTs reinforced BMG composites can be used because of their maintaining the ductility under freezing temperatures. It is envisaged that the results of this work will be used by various agencies such as national aeronautics and space administration (NASA), Indian space and research organization (ISRO), defense research and development organization (DRDO), QTech Nanosystems and United Nanotechnologies, to name a few. Some of the relevant studies related to CNT reinforced MG nanocomposites have been summarized below. This also included the latest research on the simulation of CNT reinforced MG materials. The rationale behind this was to put the present work in perspective with the state-of-the-art literature.

Endo et al. [2] performed an experimental mensuration of the elastic modulus, Poisson's ratio and deformation behavior of the SWCNTs and MWCNTs. It was concluded that the elastic modulus, Poisson's ratio and strain energy were the function of nanotube size and structure. It was also predicted that the fracture of zig-zag tube occurred at a lower strain than that of the armchair tube. Wang et al. [3] prepared CNT reinforced Zr-based MG composites and their physical and mechanical properties were investigated. The investigated composites were found to be lightweight and had improved physical and mechanical properties compared to the BMG itself. Song et al. [4] studied the mechanical behavior of CNT reinforced gold (Au) composites using molecular dynamics (MD) simulation. It was observed that the increase in stiffness of long CNT reinforced gold composites was larger than that the corresponding increase in stiffness of monolithic nano-single crystal gold matrix. Sopu et al. [5] performed MD simulations to study the deformation behavior of $Cu_{64}Zr_{36}$ structure reinforced with B_2CuZr nanowires. When the nanowires were distributed in the glassy matrix along the deformation direction, a two-step stress-induced martensitic phase transformation was observed. Sharma et al. [6] investigated the effect of CNT and graphene reinforcements on the mechanical properties of MG by using the MD simulation. The MG-graphene composites were found to have better mechanical properties in comparison to the MG-CNT composites.

Deng et al. [7] investigated the mechanical characteristics of long and short CNT reinforced MG composites by MD. The results of tensile and compressive behavior were compared with the monolithic MG. MG reinforced with short CNTs showed less increase in mechanical properties. Long CNTs dramatically improved the strength and stiffness of amorphous MGs. In contrast, the short CNTs were unable to strengthen the MG matrix. Sharma et al. [8] evaluated the mechanical and thermal properties of graphene-CNT reinforced copper matrix composites by MD. The result showed that with the increased volume fraction of nanofiller, Young's modulus as well as the thermal conductivity of single-layer graphene sheet copper composites increased at a faster rate than that for CNT-copper composites. Rezaei et al. [9] found graphene as an effective reinforcement to improve the ductility and toughness of MG composites. Srivastava et al. [10] conducted atomistic simulations and estimated the effect of CNT on the elastic and mechanical behavior of aluminium (Al) based MG composites. It was concluded that the increase in stiffness of CNT reinforced Al composite was larger than that of the monolithic Al matrix. Liu et al. [11] studied the uniaxial tensile response of CNT reinforced copper nanocomposites with MD simulations. The results showed that the CNTs strongly improved the Young's modulus and yield strength of CNT/copper nanocomposites.

Jensen et al. [12] performed MD simulation on high volume fraction continuous and discontinuous CNT reinforced amorphous carbon composites with the covalent linking fractions ranging from 0 to 20% of the outer tube atoms. It was observed that any degree of interfacial bonding had a negative impact on the axial tensile strength and stiffness. For the discontinuous composites, the modulus was maximized between 4 % and 7% interface bonding, and the strength continued to increase up to higher levels of interfacial bonding studied. Jiang et al. [13], investigated the mechanical behavior of nanocomposites consisting of highly ordered nanoporous nickel (HONN) and its CNT-reinforced composites (CNHONNs) subjected to a high temperature of 900 K by MD simulation. It was shown that the out-of-plane mechanical properties of HONN were generally superior to its in-plane mechanical properties. Compared to pure HONNs, through the addition of CNTs from 1.28 wt% to 5.22 wt%, the weight of the composite could be reduced by 5.83%–2.33%. The MD simulations provided further insights into the deformation mechanism at the atomic scale, including a fracture in tension, pore collapse in compression and local changes in lattice structures due to the stacking faults. Kumar and Haldar [14] synthesized multi-walled CNT reinforced bismuth-silicate glass composites using colloidal method. It was found that above a percolation threshold, the glass composites showed metallic behavior. A model for thermal conductivity of glass nanocomposites was also developed.

Lee et al. [15] prepared the CNT/$Ti_{50}Cu_{28}Ni_{15}Sn_7$ MG composites using vacuum hot-pressing. The prepared samples were tested for corrosion resistance by dipping in Hank's solution at 37 °C. Results showed that the Ti-based BMG composites displayed spontaneous passivity by anodic polarization with a passive current density of about 10^{-5} A/cm^2. Li et al. [16] studied the effect of Tantalum (Ta) particles on the fracture behaviour of notched BMG composites. It was found that due to high state of tri-axial stress, the shear banding was suppressed. The fracture strength was found to decrease with an increase in the volume fraction of Ta particles.

Based on the review, some of the gaps and challenges related to the CNT reinforced MG composites could be highlighted as:

i. A lot of work has been accomplished in the field of MG nanocomposites materials in the last few years, but most of the studies have been performed experimentally. Very few studies have been performed using MD.
ii. The variation of mechanical properties of CNT-MG composites with CNT volume fraction has not been investigated.
iii. The variation of thermal conductivity of CNT-MG composites with CNT volume fraction has not been predicted using MD.
iv. The effect of functionalization of SWCNT with different functional groups, on the properties of CNT reinforced MG composites has not been investigated.

The above stated research gaps have been filled with the help of this study.

2. Molecular dynamics methodology

The MD methodology has been shown in Fig. 1. All the MD simulations in this study have been performed using Biovia Materials Studio [17].

2.1. Building and packing

Firstly, Zr and Cu atoms were built with the help of the periodic

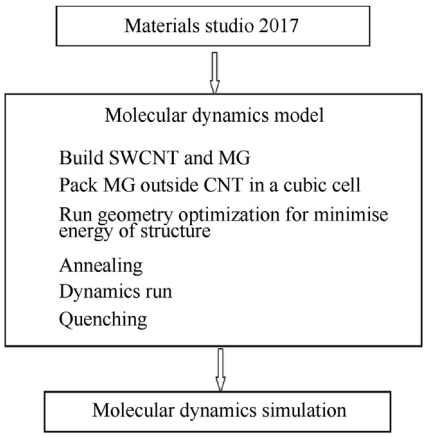

Fig. 1. Flow chart of MD methodology.

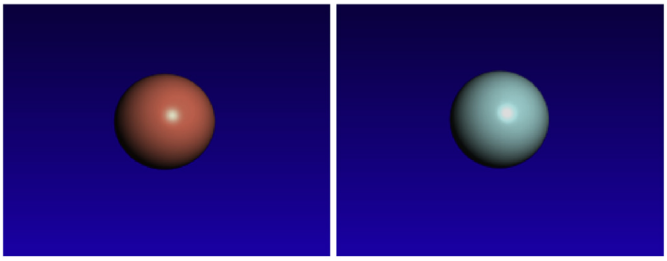

Fig. 2. Copper (Cu) and Zirconium (Zr) atoms.

table, as shown in Fig. 2. An amorphous configuration of $Cu_{64}Zr_{36}$ was created using the "Amorphous cell" module of Materials Studio 7.0. Fig. 3 shows the structure of $Cu_{64}Zr_{36}$ system having dimensions of $50 \times 50 \times 50$ Å^3 and containing a total of 8442 atoms with a density of 8 gm/cm^3. The parameters of packing have been shown in Table 1.

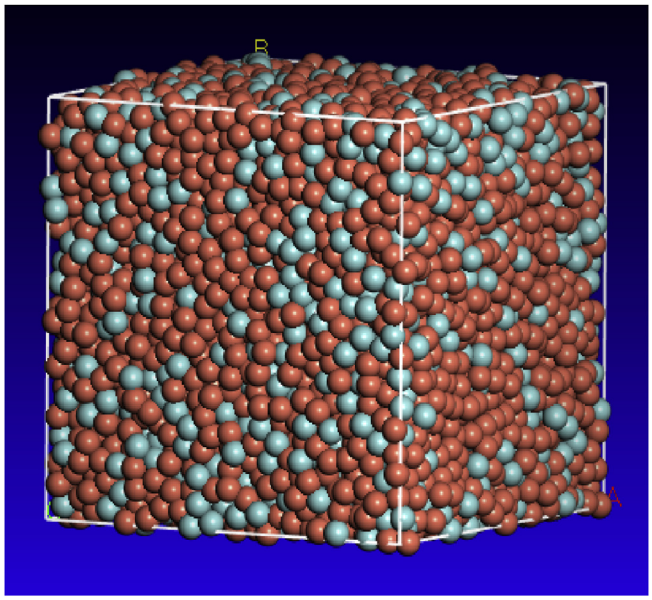

Fig. 3. Amorphous structure of $Cu_{64}Zr_{36}$ alloy having a molar ratio of Zr and Cu as.

Table 1
Packing parameters for MG and SWCNT-MG composites.

S. No.	Parameter	Value
1.	Density	8 gm·cm^{-3}
2.	Forcefield	Universal
3.	Charges	Use current
4.	Summation method	Ewald
5.	Truncation method	Cubic spline
6.	Buffer width	0.5 Å
7.	Cut off distance	12.5 Å

2.2. Geometry optimization

The initial configuration of $Cu_{64}Zr_{36}$ MG has higher energy. Hence, to bring it into an equilibrium state, the process of geometry optimization has to be performed. The parameters for geometry optimization of the MG has been shown in Table 2. If this step has not been performed and the simulation has been started directly from a non-optimed structure, erroneous results would be obtained. 'Smart' algorithm has been used for performing the process of geometry optimization. This algorithm is a combination of 'Steepest descent' and 'Conjugate gradient' algorithms.

2.3. Anneal dynamics

In this step, the temperature was increased periodically from an initial temperature to a mid-cycle temperature and then returned to its original temperature. After the end of each cycle, a structure with the lowest energy was obtained. This structure was then exported to a standard trajectory file. Annealing involves a series of isothermal stages, each stage involving a prescribed number of dynamics steps. After each temperature cycle, the velocity scaling of the atoms was performed to modify the kinetic energy of the structure. This led to a change in the temperature. Then the cycle is repeated at this new temperature and a number of dynamics steps were performed again. On the completion of the anneal dynamics, the anneal trajectory was exported to a study table for the identification of the structure having the lowest energy. The temperature increment between each isothermal stage of an annealing cycle is dictated by the initial and mid-cycle temperature and also by the heating ramps per cycle. The number of dynamics steps to be performed at each constant-temperature stage also needs to be specified. The total number of temperature changes per anneal cycle is twice the number of heating ramps per cycle (increasing the temperature and then decreasing it again). Thus, the total number of dynamics steps performed during an anneal dynamics calculation is given by:

$$\begin{aligned}(\text{Total steps}) &= (\text{Number of cycles}) \\ &\times 2(\text{Number of ramps per cycle}) \\ &\times (\text{Number of steps per ramp})\end{aligned}$$

The parameters of anneal dynamics have been given in Table 3.

Table 2
Geometry optimization parameters for MG and SWCNT-MG composites.

S. No.	Parameter	Value
1	Algorithm	Smart
2	Quality	Fine
3	Energy tolerance convergence	10^{-4} kcal mol^{-1}
4	Force tolerance convergence	0.005 kcal mol^{-1} Å^{-1}
5	Distance tolerance convergence	5×10^{-5} Å
6	Maximum number of iterations	5000

Table 3
Anneal dynamics parameters for MG and SWCNT-MG composites.

S. No.	Parameter	Value
1	Initial temperature	300 K
2	Mid-cycle temperature	2000 K
3	Heating ramps per cycle	5
4	Dynamics step per ramp	100
6	Maximum number of iterations	5000

2.4. Forcite dynamics

After an optimized structure has been obtained, the structure could be subjected to a dynamics run. In this step, the effects of pressure and temperature on the structure are considered. The output of dynamics run is a trajectory file that contains useful information about the configuration and velocities of atoms. Constant number of atoms, volume, and energy ensemble (NVE) has been used in this study. For controlling the temperature and pressure, Andersen's thermostat [18] and Berendsen barostat [19] were used. The parameters used in the simulation have been tabulated in Table 4. The details of Forcite dynamics could be found in another work by the authors [8].

2.4.1. Andersen's thermostat

The temperatures calculated from the translational and angular velocities of particles are denoted by $T_{cal}^{(t)}$ and $T_{cal}^{(r)}$, respectively, and written as;

$$T_{cal}^{(t)} = \frac{1}{3N}\sum_{i=1}^{N}\frac{mv_i^2}{k}, T_{cal}^{(r)} = \frac{1}{3N}\sum_{i=1}^{N}\frac{I\omega_i^2}{k} \quad (1)$$

Where, N is the total number of particles, assumed to be $N \gg 1$. $T_{cal}^{(t)}$ and $T_{cal}^{(r)}$ calculated from v_i and ω_i (i = 1, 2, …, N), are generally not equal to the desired temperature T. This equilibration procedure adjusts temperatures calculated from the translational and angular velocities of particles to T during the simulation by using the method of scaling the translational and angular velocities of each particle. If $T_{cal}^{(t)ave}$ and $T_{cal}^{(r)ave}$ denote the averaged values of $T_{cal}^{(t)}$ and $T_{cal}^{(r)}$ taken, for example, over 50 time steps, then the scaling factors $c_0^{(t)}$ and $c_0^{(r)}$ can be determined as;

$$c_0^{(t)} = \sqrt{\frac{T}{T_{cal}^{(t)ave}}}, \; c_0^{(r)} = \sqrt{\frac{T}{T_{cal}^{(r)ave}}} \quad (2)$$

With the scaling factors determined, the translational and angular velocities of all particles in a system can be scaled as;

Table 4
Dynamics parameters for MG and SWCNT-MG composites.

S. No.	Parameter	Value
1	Ensemble	NVE
2	Initial velocity	Random
3	Temperature	300
4	Time step	1 fs
5	Total simulation time	100
6	Number of steps	1,00,000
7	Frame output every	5000
8	Thermostat	Andersen
9	Collision ratio	1
10	Energy deviation	5×10^{12} kcal/mol
11	Repulsive cut-off	6 Å

$$\boldsymbol{v}_i' = c_0^{(t)}\boldsymbol{v}_i \;, \; \omega_i' = c_0^{(r)}\omega_i \qquad (i = 1, 2, \ldots\ldots, N) \quad (3)$$

This treatment yields the desired system temperature T.

2.4.2. Berendsen barostat

The Berendsen barostat is a method for controlling the pressure in a MD simulation. The Berendsen barostat adds an extra term to the equations of motion which effects the pressure change.

$$\frac{dP(t)}{dt} = \frac{1}{\tau}(P_0 - P(t)) \quad (4)$$

Where, P_0 is the reference pressure and P is the instantaneous pressure, τ is the coupling parameter which determines how tightly the bath and the system are coupled together. This method gives an exponential decay of the system towards the desired pressure.

Thus, the scaling factor can be writtens as;

$$\lambda = 1 - \frac{K_T\delta t}{3\tau}(P_0 - P(t)) \quad (5)$$

Where, K_T is the isothermal compressibility = 4.6×10^{-5} bar^{-1}.

The system was performing approximately 100000 steps when the temperature was stabilized using the Andersen's thermostat. The time step was taken as 1 fs. Similarly, constant no. of atoms, pressure and temperature (NPT) ensemble was used for stabilizing the pressure. The number of steps were specified as 100000 with a time step of 1 fs.

2.5. Quench dynamics

Quench dynamics alternates periods of a dynamics simulation with a quench period in which the structure is minimized. This provides a means of searching conformational space for low energy structures. Between quenches, a standard dynamics simulation proceeds. The interval between quenches is specified when the job is set up. When a quench point is reached, the current structure is copied and output to the standard trajectory file. The copy is then minimized using the current geometry optimization parameters, and the minimized structure is output to the quench trajectory file. After the quench process has been completed, the dynamics simulation continues from the unquenched structure. On completion of the quench dynamics simulation; the quench trajectory is loaded into a study table for simple analysis and identification of the low energy conformations. Standard dynamics analysis may be performed on either of the trajectories, although techniques assuming standard time evolution of the trajectory are disabled for the quench trajectory. The parameters of quench dynamics have been shown in Table 5. The same procedure as specified in Section 2.5 was adopted for controlling the pressure and temperature.

2.6. Mechanical properties

Before calculating the mechanical properties, quench dynamics

Table 5
Forcite quench dynamics parameters for MG and SWCNT-MG composites.

S. No.	Parameter	Value
1	Temperature	10 K
2	Pressure	0.0 GPa
3	Time step	1 fs
4	Total simulation time	100 ps
5	Number of steps	100000
6	Quench steps every	5000

was performed to achieve the amorphous structure of $Cu_{64}Zr_{36}$. Quench dynamics was preceded by the anneal dynamics and dynamics run. After quench dynamics, the final amorphous structure of the CNT reinforced $Cu_{64}Zr_3$ was obtained. A stress-strain script has been written using the 'Perl Script' module of Biovia Materials Studio to calculate the mechanical properties. Input stresses and universal force field were given as the input parameters in the stress-strain script to calculate the mechanical properties. A sequence of stresses were applied on each structure followed by an equilibration and production stage. The stresses were applied along the length of the CNT. The stress-strain script could be found in a supplementary file provided with this work (Appendix A.1).

2.7. Thermal conductivity

Thermal conductivity has been predicted by using the thermal conductivity script written using the 'Perl Script' module of Biovia Materials Studio [17]. The details of the script could be found in the supplementary file provided with this work (Appendix A.2). In this study, the script for calculating the thermal conductivity has been written based on the imposed flux method of Jund [20]. The thermal conductivity was predicted by giving the user input parameters such as, xsd file name, force field, and thermostat. In this study, universal force field (UFF) and Nose thermostat have been used. The details of the imposed flux method could be found in another work by the authors [8]. While the energy spectrum of molecular vibrations encompass a relatively large frequency range, high-frequency vibrations tend to be spatially localized and energetically above the cutoff frequency of many solid-state substrates. For these reasons, and also because such modes are not populated at room temperature, they contribute little to molecular heat transport at that temperature [21]. Molecular heat transport is therefore dominated by lower frequency vibrations, for which classical dynamics provide a reasonable approximation. Molecular Force-Fields (FF) allow efficient representation of a classical, anharmonic molecular potential energy surface which is the input to the stochastic non-equilibrium MD (SNEMD) studies. Hence UFF can predict the thermal conductivity of CNT/MG composites. To find the thermal conductivity, MD simulations were performed with CNT volume fractions varying from ($V_f = 0$–0.12). Results of thermal conductivity obtained using MD simulations were compared with other models such as the series model, Maxwell-Garnett model, and Hamilton-Crosser model. The details of these models could be found in another work of the authors [8].

2.8. CNT- $Cu_{64}Zr_{36}$ composite

An armchair (6,6) CNT was constructed using the "build nanostructure" tool in Biovia Materials Studio. Fig. 4 shows the armchair (6,6) CNT having a length of 39.35 Å. The CNTs were then packed inside the MG matrix using the "amorphous" module, as shown in Fig. 5. The mechanical properties of SWCNT-MG composites were investigated and compared with the pure MG. The effect of increasing the volume fraction of the SWCNT on the mechanical properties of the composites was studied. The same procedure, as discussed in the previous sections, was adopted.

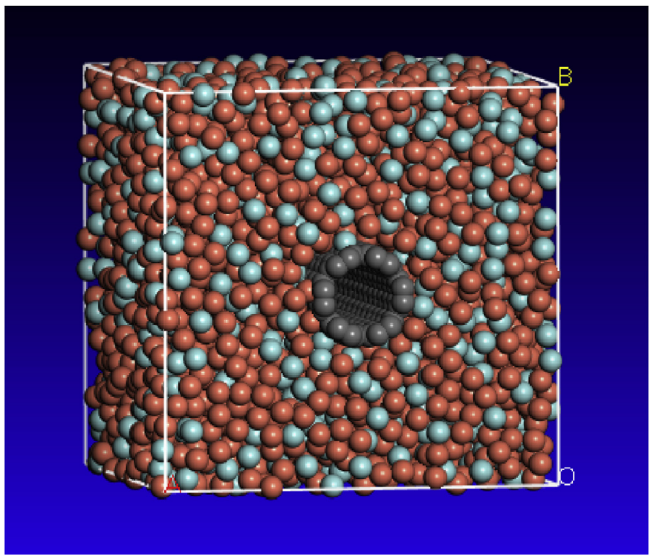

Fig. 5. MG ($Cu_{64}Zr_{36}$) reinforced with SWCNT (front view).

2.9. Functionalized CNT reinforced MG composite

The influence of functionalization of SWCNT on the mechanical properties has also been predicted using MD. This study analyzes the effect of carboxylic (-COOH), ester (-$COOCH_3$) and vinyl (-$CH{=}CH_2$) groups attached on the surface of armchair (4,4) SWCNT on the mechanical properties of $Cu_{64}Zr_{36}$ composites. Fig. 6 shows the ester, vinyl and carboxylic groups modeled using Biovia Materials Studio. Calculations have been made for different volume fraction of functionalized CNTs. Elastic properties of SWCNT–MG composites have also been simulated for a varying number of functional groups. The same procedure, as discussed earlier in previous sections, was adopted. Fig. 7 shows an armchair (4,4) SWCNT functionalized with 12 molecules of the vinyl group. Fig. 8 shows a vinyl-functionalized SWCNT packed in $Cu_{64}Zr_{36}$ matrix with 2161

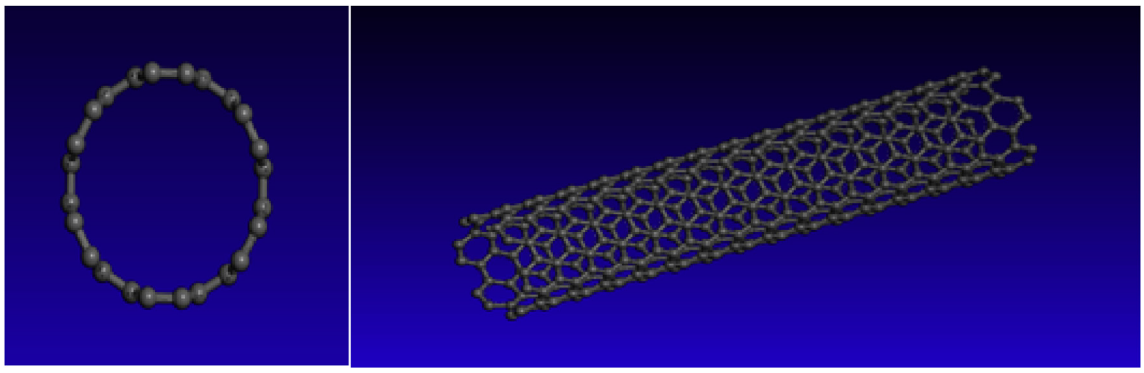

Fig. 4. An armchair (6,6) SWCNT with a diameter of 8.14 Å and length of 39.35 Å.

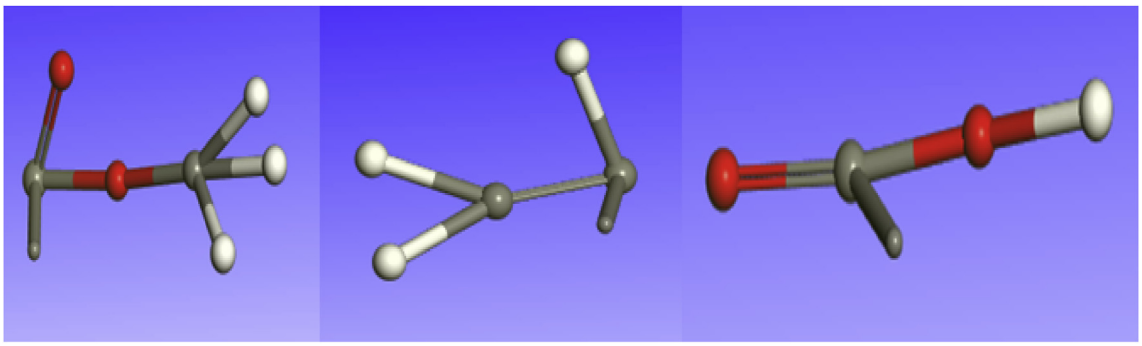

Fig. 6. (a) Ester, (b) Vinyl, (c) Carboxylic, functional groups modeled using Biovia Materials Studio.

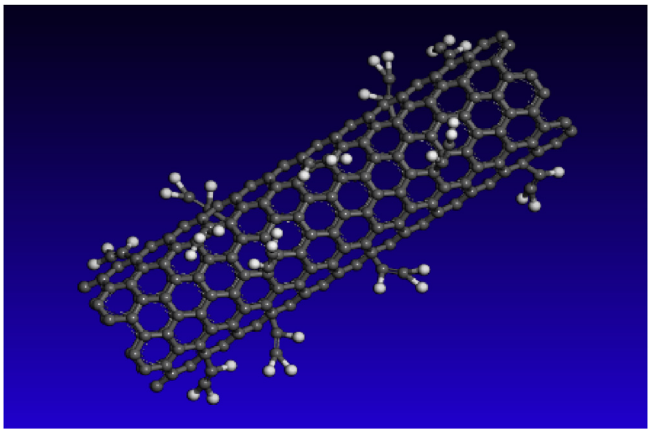

Fig. 7. Functionalized SWCNT with 12 molecules of vinyl group.

atoms. Fig. 9 shows an armchair (4,4) SWCNT functionalized with 12 molecules of ester group and Fig. 10 shows an ester-functionalized SWCNT packed in $Cu_{64}Zr_{36}$ matrix with 2171 atoms. Fig. 11 shows an armchair (4,4) SWCNT functionalized with

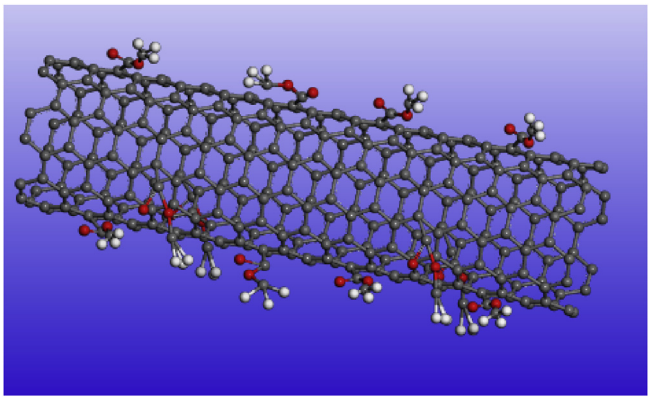

Fig. 9. Functionalized SWCNT with 12 molecules of ester group.

12 molecules of the carboxylic group and Fig. 12 shows a carboxylic functionalized SWCNT packed in $Cu_{64}Zr_{36}$ matrix with 2164 atoms. Similarly, the (6,6) SWCNT functionalized with 2, 4, 8, and 12 cross-links was modeled.

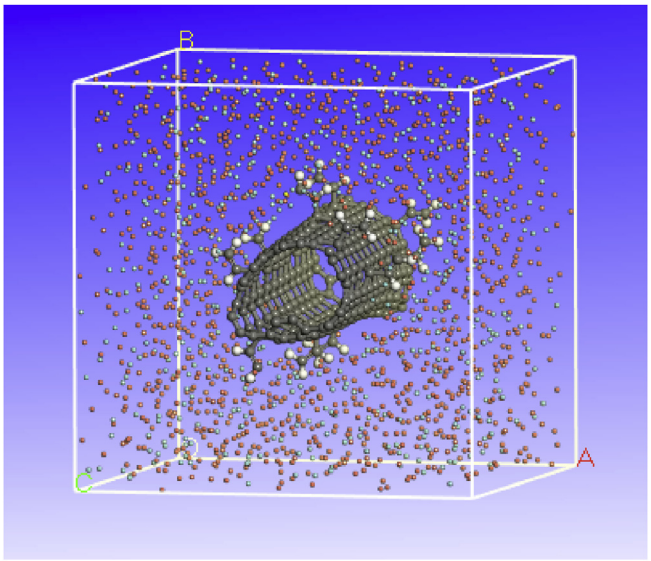

Fig. 8. Vinyl functionalized SWCNT packed in MG matrix with.

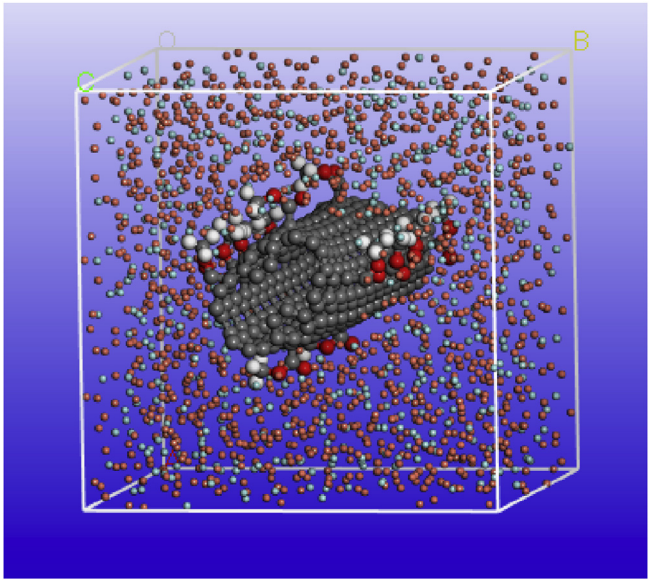

Fig. 10. Ester functionalized SWCNT packed in MG matrix with 2171 atoms.

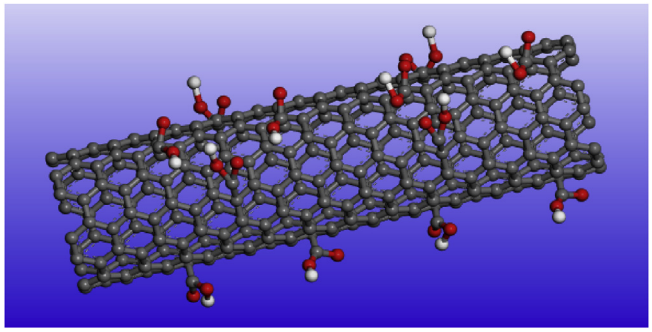

Fig. 11. Functionalized SWCNT with 12 molecules of carboxylic group.

3. Results and discussion

This section shows the results of CNT reinforced $Cu_{64}Zr_{36}$ composites, which were obtained from the MD simulation using Biovia Materials Studio. Three cases, MG, SWCNT- MG composites and functionalized SWCNT-MG composites were considered. In this study, simulations were performed to predict the mechanical and thermal properties for all three cases.

3.1. Properties of $Cu_{64}Zr_{36}$ MG

In the first step, the pure $Cu_{64}Zr_{36}$ MG was analysed. The size of the computational cell was 50 Å × 50 Å × 50 Å and containing a total of 8442 atoms (Fig. 3). The Young's modulus of MG was found to be 58.07 GPa at a temperature of 300 K which is in agreement with the value of 60.3 GPa reported by Sharma et al. [6] and 59.4 GPa Deng et al. [7]. Additionally, the yield strength and the corresponding strain of the MG were obtained as 2.24 GPa and 2.7%, respectively. This strength was defined as the stress at which the yielding of MG appeared, following a significant reduction in the measured stress. Table 6 shows the results for the mechanical properties of pure MG specimen and Table 7 shows the thermal conductivity of the pure MG.

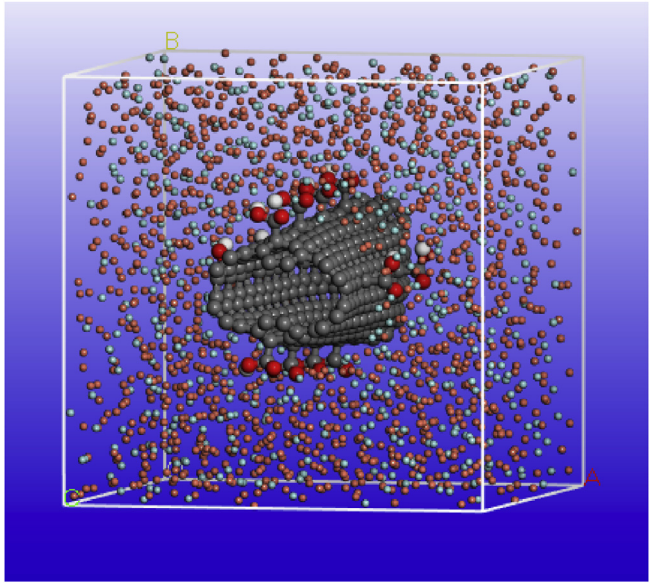

Fig. 12. Carboxylic functionalized SWCNT packed in MG matrix with 2164 atoms.

Table 6
Comparison of mechanical properties of MG obtained from the present study with those available in the literature.

Study	E/GPa	σ_y /GPa	ε_y
Sharma et al. [6]	60.3	2.4	0.045
Deng et al. [7]	59.4	2.55	0.06
Present study	58.07	2.24	0.027

Table 7
Comparison of thermal conductivity (K) of MG obtained from the present study with those available in the literature.

Study	MG	K/(W·mK^{-1})
Yamasaki et al. [22]	$Zr_{41}Ti_{14}Cu_{12}Ni_{10}Be_{23}$	4.5
Umetsu et al. [23]	$Zr_{55}Al_{10}Cu_{35}$	3.9
Present study	$Cu_{64}Zr_{36}$	1.52

3.2. Effect of volume fraction of CNT

An armchair (6, 6) SWCNT with diameter 8.14 Å and length 39.95 Å was reinforced in $Cu_{64}Zr_{36}$ MG matrix with different volume fractions. The result shows that by increasing the V_f of SWCNTs in MG matrix, the Young's modulus of the composites increased. This increase in Young's modulus of the composites was attributed to the high-value of stiffness of the CNT reinforcement. The values of Young's modulus were 78.95 GPa, 81.3 GPa, 99.2 GPa and 111.11 GPa at 3%, 5%, 8% and 12% V_f of CNTs as shown in Fig. 13. From Fig. 13, it could be observed that at lower values of V_f (from 0 to 5%), the percentage increase in Young's modulus was approximately 66%. As the value of V_f was increased further (from 5 % to 12%), the rate of increase in Young's modulus was only 16%. This could be attributed to agglomeration of CNTs at high values of V_f, which could lead to a drastic fall in the rate of increase of Young's modulus of CNT-MG composite. The increase in the values of Young's modulus was comparable with the results obtained by Sharma et al. [6] and Deng et al. [7]. The comparison has been shown in Table 8. Thus, it could be stated that the results of this study are in agreement with the literature.

3.3. Thermal conductivity

A script has been written in Biovia Materials Studio for

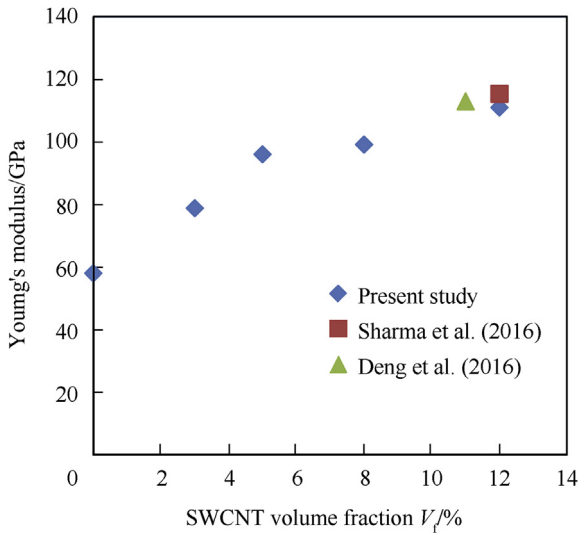

Fig. 13. Variation of elastic modulus (E_{11}) of SWCNT-MG with SWCNT.

Table 8
Comparison of Young's modulus of SWCNT-MG with those available in the literature.

Study	V_f	E/GPa
Sharma et al. [6]	12%	115.5
Deng et al. [7]	11%	113
Present study	12%	111.11

predicting the thermal conductivity of the composites. Thermal conductivity of SWCNT-MG composites increased with increasing the SWCNT V_f. Fig. 14 shows the value of thermal conductivities at different CNT volume fractions.

The thermal conductivity was found to increase from 1.52 W/mK at $V_f = 0\%$ to 5.88 W/mK at $V_f = 12\%$, thus giving an increase of approximately 286%. The percentage difference between the values of thermal conductivity obtained from MD and other models has been shown in Table 9. The series model was found to give the lowest values of thermal conductivity. This could be attributed to the fact that in series model, the interaction between the CNT and the MG matrix has been presumed to be negligible. Thus, the series model gave the lower bound of thermal conductivity. The Maxwell-Garnett model predicted the thermal conductivity to be slightly higher than that given by the series model. This model gave satisfactory results at low values of V_f but at higher values, it has been found to give erroneous results. The Hamilton-Crosser model also takes into consideration the non-sphericity of the CNT and predicted the values of thermal conductivity to be higher than that given by the Maxwell-Garnett model and series model.

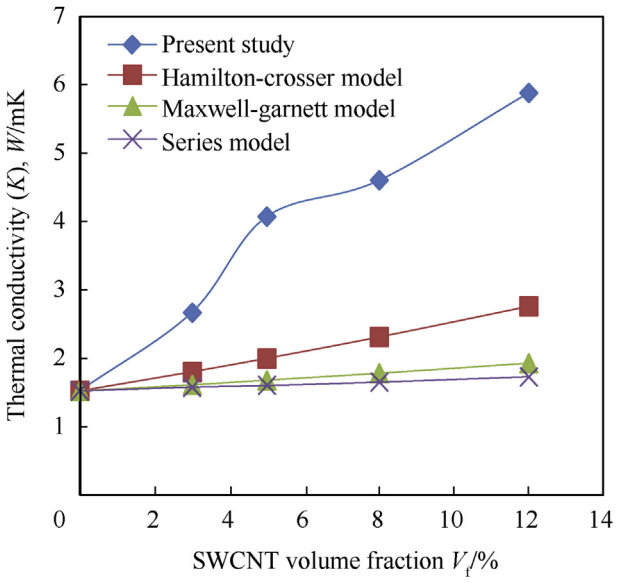

Fig. 14. Comparison of MD results of thermal conductivity for CNT-reinforced MG composites with other models.

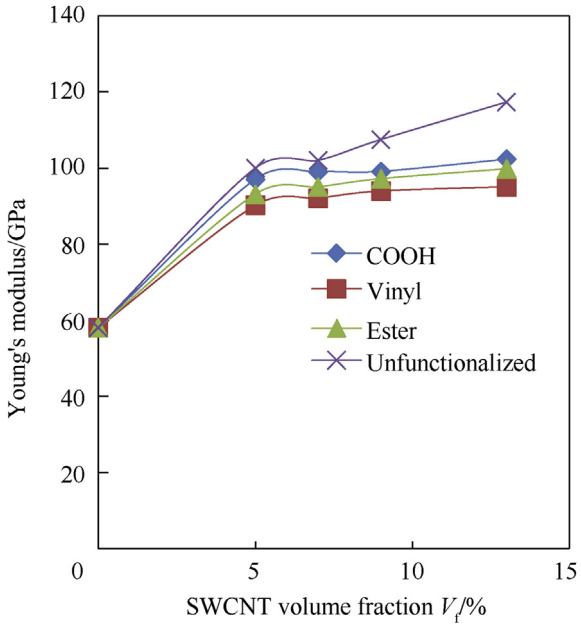

Fig. 15. Variation of Young's modulus (E_{11}) with SWCNT volume fraction (V_f) for fixed aspect ratio of CNT ($l/d = 4$) and three functional groups.

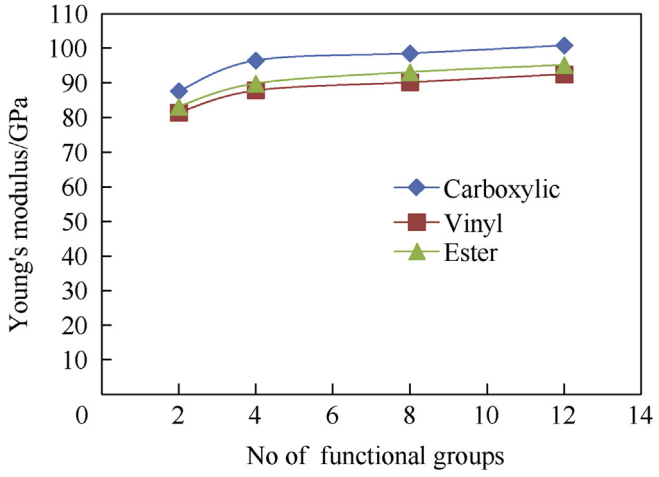

Fig. 16. Variation of Young's modulus (E_{11}) with number of functional groups for the fixed aspect ratio of CNT ($l/d = 4$) and volume fraction ($V_f = 0.05$).

3.4. Effect of functionalization of CNTs

3.4.1. Young's modulus

In CNT every carbon atom consists of sp^2 hybridization due to the double bonding between C-C atoms, but when functional groups are attached to carbon on the surface of SWCNT,

Table 9
Comparison of thermal conductivity of SWCNT-MG composite obtained from MD with other models.

SWCNT V_f /%	Thermal conductivity (K)/(W·mK^{-1})			
	MD	Hamilton-Crosser model	Maxwell-Garnett model	Series model
0	1.52	1.52	1.52	1.52
6	4.2	2.10	1.70	1.60
12	5.88	2.80	1.90	1.80

Table 10
Percentage rise in Young's modulus (E_{11}) with the number of functional groups for fixed volume fraction ($V_f = 0.05$) and aspect ratio ($l/d = 4$) of SWCNT.

Increase in the number of functional groups	% increase in Young's modulus for		
	COOH functionalized SWCNT-MG composite	$COOCH_3$ functionalized SWCNT-MG composite	CH_2=CH functionalized SWCNT-MG composite
2–12	15.05%	15.92%	13.55%

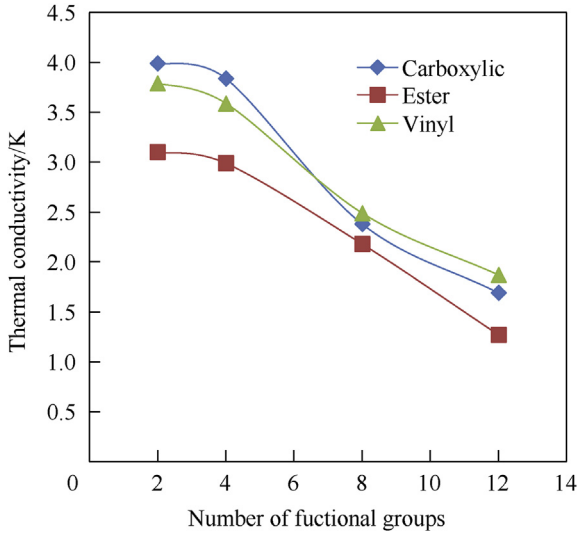

Fig. 17. Variation in thermal conductivity (K) with the number of functional groups for fixed aspect ratio ($l/d = 4$) and SWCNT volume fraction ($V_f = 0.09$).

hybridization changes to sp^3. This change in sp^2 to sp^3 hybridization of surface carbon distorts the structure of CNTs leading to a change in their properties. Fig. 15 shows the variation of Young's modulus (E_{11}) with SWCNT V_f for fixed aspect ratio ($l/d = 4$) and three groups attached with SWCNT. It could be seen that the functionalization reduced the values of E_{11}. The decrease in E_{11} of functionalized SWCNT-MG composite concerning pristine SWCNT-MG composite was the largest for vinyl (CH_2=CH) functionalized SWCNT reinforced MG composites due to weak hydrogen bonding. The change in hybridization from sp^2 to sp^3 weakens the chemical bonds in the vicinity of the functionalization, leading to the reduction in the Young's modulus. A similar reduction in E_{11} was observed for ester ($COOCH_3$) and carboxylic (COOH) groups, as could be observed from Fig. 15.

Fig. 16 shows the variation of E_{11} with several functional groups for the fixed aspect ratio ($l/d = 4$) and SWCNT volume fraction ($V_f = 0.05$). It could be observed that E_{11} increases with an increase in the number of functional groups. Carboxyl (COOH) functionalized CNT reinforced MG composite exhibited the highest modulus while vinyl (CH_2=CH) functionalized CNT reinforced MG composite displayed the lowest values of E_{11}. The values of elastic modulus for ester ($COOCH_3$) functionalized CNT lie between the values of E_{11} for carboxylic (COOH) and vinyl (CH_2=CH) functionalized CNT reinforced MG composites. Table 10 shows the percentage rise in E_{11} with the number of functional groups for the fixed aspect ratio ($l/d = 4$) and volume fraction ($V_f = 0.05$) of SWCNT. Ester ($COOCH_3$) functionalized CNT reinforced MG composite showed the biggest improvement in Young's modulus E_{11} while vinyl (CH_2=CH) functionalized CNT reinforced MG composite showed the lowest percentage increase in E_{11}. The trends obtained with the help of MD simulation for an increase in the Young's modulus with an increase in SWCNT volume fraction were found to be comparable with the trends obtained by Sharma et al. [6] and Odegard et al. [24].

3.4.2. Thermal conductivity

It has been discussed in Section 3.3 that the thermal conductivity was more influenced by the interfacial zone than by the matrix material and nanofiller. Functionalization of SWCNT reduced the thermal conductivity of the SWCNT-MG composites, as shown in Fig. 17. This reduction in thermal conductivity of the functionalized SWCNT reinforced MG composites could be because of two factors. Firstly, the introduction of hydrogen atoms leading to single bonds or sp^3 bonds. Secondly, the conversion of sp^2 hybridization into sp^3 hybridization created defects, thus reducing the mean free path of the phonons.

From Fig. 17 and Table 11, it could be seen that the percentage decrease in thermal conductivity (K) with the number of functional groups for fixed volume fraction ($V_f = 0.05$) and aspect ratio ($l/d = 4$) of SWCNT was the highest for COOH functionalized SWCNT-MG composites and the least for CH_2=CH functionalized SWCNT-MG composites. Fig. 18 shows the variation in the thermal conductivity (K) of SWCNT-MG composites with increasing SWCNT volume fraction (V_f) for fixed ration ($l/d = 4$) and three functional groups carboxylic (COOH), ester ($COOCH_3$) and vinyl (CH_2=CH) with SWCNT. The thermal conductivity of the composites increased with the SWCNT volume fraction, as shown in Fig. 18. This increase in thermal conductivity was due to the excellent thermal conductivity of the individual CNTs (3000 W/mK) Yu et al. [25].

4. Conclusion

In this study, MD simulations were performed to investigate the effect of CNT reinforcement on the mechanical and thermal properties of $Cu_{64}Zr_{36}$ MG. The effect of functionalized SWCNT reinforcement on the properties of MG was also studied via MD simulation using Biovia Materials Studio 2017. The main findings have been listed below.

Table 11
Percentage decrease in thermal conductivity (K) with the number of functional groups for fixed volume fraction ($V_f = 0.05$) and aspect ratio ($l/d = 4$) of SWCNT.

Increase in the number of functional groups	% decrease in thermal conductivity for		
	COOH functionalized SWCNT-MG composite	$COOCH_3$ functionalized SWCNT-MG composite	CH_2=CH functionalized SWCNT-MG composite
2–12	29.04%	12.82%	9.15%

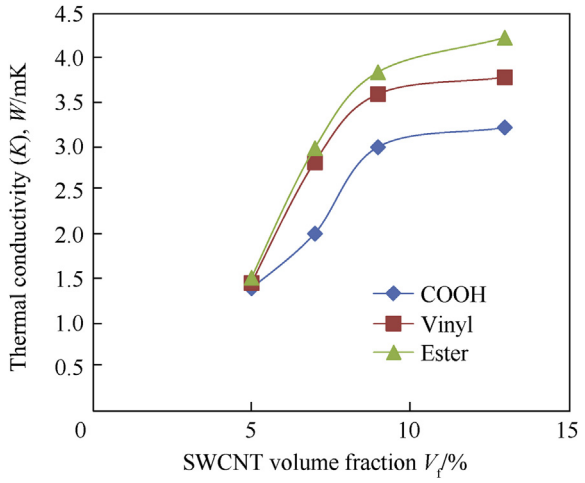

Fig. 18. Variation in thermal conductivity (K) with SWCNT volume fraction (V_f) for fixed aspect ratio ($l/d = 4$) and three functional groups attached with SWCNT.

i. Young's modulus (E_{11}) of the SWCNT-MG composites was found to be increasing with an increase in the SWCNT volume fraction (V_f). The increase in the Young's modulus were 78.95 GPa, 81.3 GPa, 99.2 GPa and 111.11 GPa at 3%, 5%, 8% and 12% volume fraction (V_f) of CNTs.
ii. The thermal conductivity of the SWCNT-MG composites was found to be increasing with an increase in the SWCNT reinforcement. Thermal conductivities at different SWCNT fraction were 1.52 W/mK at 0%, 2.67 W/mK at 3%, 4.07 W/mK at 5%, 4.60 W/mK at 8% and 5.88 W/mK at 12%.
iii. Functionalization of SWCNT with different groups led to a decrease in Young's modulus of SWCNT-MG composites. But with an increase in the percentage of functionalization, Young's modulus of the composites showed an increasing trend.
iv. The Young's modulus (E_{11}) of the functionalized SWCNT-MG composites increased with increase in the volume fraction of the SWCNT. Ester ($COOCH_3$) functionalized CNT reinforced MG showed the highest while vinyl (CH_2=CH) functionalized CNT reinforced MG composite showed the lowest percentage increase in E_{11} with functionalization.
v. Thermal conductivity of the functionalized SWCNT-MG composites decreased with an increase in the percentage of the functionalization. But with an increase in the SWCNT volume fraction, the thermal conductivity of the functionalized SWCNT-MG composites was found to increase. Carboxylic (COOH) gave the highest and vinyl (CH_2=CH) showed the lowest decrease in K with functionalization.

These findings will be immense help in the designing of CNT reinforced MG materials for use in space applications. The study can be further extended by using the coarse graining procedure as was developed by Rabczuk et al. [26,27]. A characteristic feature of the coarse grain model is the ability to capture the covalent interactions between polymer chains, and nanotubes and polymer matrix. Thus, this model can be used to predict the properties of CNT-MG composites.

Data availability

- The raw/processed data required to reproduce these findings cannot be shared at this time due to technical or time limitations. Data will be made available on request.

Declaration of competing interest

The authors declare that they have no known competing financial interests or personal relationships that could have appeared to influence the work reported in this paper.

Acknowledgement

The authors are highly grateful to the Department of Materials Science and Engineering of IIT Kanpur for providing the computational facilities for this research.

Appendix A. Supplementary data

Supplementary data to this article can be found online at https://doi.org/10.1016/j.dt.2020.04.004.

References

[1] Klement W, Willens RH, Duwez POL. Non-crystalline structure in solidified gold–silicon alloys. Nature 1960;187(4740):869.
[2] Natsuki T, Tantrakarn K, Endo M. Effects of carbon nanotube structures on mechanical properties. Appl Phys A 2004;79(1):117–24.
[3] Bian Z, Wang RJ, Wang WH, Zhang T, Inoue A. Carbon nanotube reinforced Zr-based bulk metallic glass composites and their properties. Adv Funct Mater 2004;14(1):55–63.
[4] Yang SY, Zha XW. Molecular dynamics study of mechanical properties of carbon nanotube-embedded gold composites. Phys B Condens Matter 2008;403(4):559–63.
[5] Şopu D, Ritter Y, Gleiter H, Albe K. Deformation behavior of bulk and nanostructured metallic glasses studied via molecular dynamics simulations. Phys Rev B 2015;83:100202 (R).
[6] Sharma S, Chandra R, Kumar P. Graphene/carbon nanotube reinforced metallic glass composites: a molecular dynamics study. Int J Multiscale Comput Eng 2016;14(6):555–84.
[7] Deng C, Reza R, Shariati M, Tavakoli-Anbaran H. Mechanical characteristics of CNT-reinforced metallic glass nanocomposites by molecular dynamics simulations. Comput Mater Sci 2016;119:19–26.
[8] Sharma S, Kumar P, Kumar N, Chandra R. "Graphene/carbon nanotube reinforced nickel composites: a molecular dynamics study. Compos Mech Comput Appl An Int J 2018. https://doi.org/10.1615/CompMechComputApplIntJ.2018021097.
[9] Reza R, Deng C, Shariati M, Tavakoli-Anbaran H. The ductility and toughness improvement in metallic glass through the dual effects of graphene interface. J Mater Res 2017;32(2):392–403.
[10] Srivastava AK, Mokhalingam A, Singh A, Kumar D. Molecular dynamics study of mechanical properties of carbon nanotube reinforced aluminum composites. AIP Conf Proc 2016;1728(1):020297.
[11] Liu S, Yuping Y, Lei Y. Tensile responses of carbon nanotubes-reinforced copper nanocomposites: molecular dynamics simulation. Comput Mater Sci 2018;151:273–7.
[12] Jensen BD, Odegard GM, Kim JW, Sauti G, Siochi EJ, Wise KE. Simulating the effects of carbon nanotube continuity and interfacial bonding on composite strength and stiffness. Compos Sci Technol 2018;166:10–9.
[13] Jiang WG, Yu Z, Li DS, Qin QH. Study on lightweight and strengthening effect of carbon nanotube in highly ordered nanoporous nickel: a molecular dynamics study. Appl Sci 2019;9(2):352.
[14] Kumar VVRK, Haldar T. Broadband dielectric behavior of the multiwall carbon nanotube-bismuth silicate glass-nanocomposites. J Alloys Compd 2019;772:218–29.
[15] Lee PY, Hsu CF, Kai W, Lin HM, Lin CK. Fabrication and corrosion behavior of Ti-based bulk metallic glass composites containing carbon nanotubes. J Alloys Compd 2010;504:176–S179.
[16] Li Y, Pan J, Lin Y, Zhang J, Huang W. Effect of Ta particles on the fracture behavior of notched bulk metallic glass composites. Intermetallics 2019;106:1–6.
[17] Dassault Systèmes BIOVIA. Materials Studio, 7.0. San Diego: Dassault Systèmes; 2017.
[18] Andersen HC. Molecular dynamics simulations at constant pressure and/or temperature. J Chem Phys 1980;72(4):2384.
[19] Berendsen HJC, Postma JPM, van Gunsteren WF, DiNola A, Haak JR. Molecular dynamics with coupling to an external bath. J Chem Phys 1984;81:3684–90.
[20] Jund P, Jullien R. Molecular dynamics calculation of the thermal conductivity of vitreous silica. Phys Rev B 1999;59:13707–11.
[21] Sharony I, Chen R, Nitzan A. Stochastic simulation of nonequilibrium heat conduction in extended molecule junctions. Condensed Matter-Materials Science; 2019, 08617. arXiv:1908.
[22] Yamasaki M, Kagao S, Kawamura Y. Thermal diffusivity and conductivity of Zr55Al10Ni5Cu30 bulk metallic glass. Scripta Mater 2005;53(1):63–7.
[23] Umetsu RY, Tu R, Goto T. Thermal and electrical transport properties of Zr-

based bulk metallic glassy alloys with high glass-forming ability. Mater Trans 2012;53(10):1721–5.
[24] Odegard GM, Frankland SJV, Harik VM, Brenner DW, Gates TS. The stress–strain behavior of polymer–nanotube composites from molecular dynamics simulation. Compos Sci Technol 2003;63(11):1655–61.
[25] Yu C, Shi L, Yao Z, Li D, Majumdar A. Thermal conductance and thermopower of an individual single-wall carbon nanotube. Nano Lett 2005;5(9):1842–6.
[26] Rabczuk T, Arash B, Park HS. Coarse-grained model of the J-integral of carbon nanotube reinforced polymer composites. Carbon 2016;96:1084–92.
[27] Rabczuk T, Mousavi AA, Arash B, Zhuang X. A coarse-grained model for the elastic properties of cross linked short carbon nanotube/polymer composites. Compos B Eng 2016;95:404–11.